

1 Within-host diversity improves phylogenetic and transmission
2 reconstruction of SARS-CoV-2 outbreaks

3 Arturo Torres Ortiz¹, Michelle Kendall², Nathaniel Storey³, James Hatcher³,
4 Helen Dunn³, Sunando Roy⁴, Rachel Williams⁵, Charlotte Williams⁵, Richard
5 A. Goldstein⁵, Xavier Didelot², Kathryn Harris^{3,6}, Judith Breuer⁴, Louis
6 Grandjean^{4*}

7 ¹ Department of Infectious Diseases, Imperial College London, London, W2 1NY

8 ² Department of Statistics, University of Warwick, Coventry, CV4 7AL

9 ³ Department of Microbiology, Great Ormond Street Hospital, London WC1N 3JH

10 ⁴ Department of Infection, Immunity and Inflammation, Institute of Child Health, UCL,
11 London WC1N 1EH

12 ⁵ UCL Genomics, Institute of Child Health, UCL, London WC1N 1EH

13 ⁶ Department of Virology, East South East London Pathology Partnership, Royal London
14 Hospital, Barts Health NHS Trust, London E12ES

15
16 *Corresponding author l.grandjean@ucl.ac.uk

17 Institute of Child Health, 30 Guilford Street, London, WC1N 1EH

18 **Keywords:** Phylogenetics, within-host diversity, transmission, infectious diseases, SARS-
19 CoV-2

20 Abstract

21 Accurate inference of who infected whom in an infectious disease outbreak is critical for the
22 delivery of effective infection prevention and control. The increased resolution of pathogen
23 whole-genome sequencing has significantly improved our ability to infer transmission events.
24 Despite this, transmission inference often remains limited by the lack of genomic variation
25 between the source case and infected contacts. Although within-host genetic diversity is com-
26 mon among a wide variety of pathogens, conventional whole-genome sequencing phylogenetic
27 approaches to reconstruct outbreaks exclusively use consensus sequences, which consider only
28 the most prevalent nucleotide at each position and therefore fail to capture low frequency
29 variation within samples. We hypothesized that including within-sample variation in a phy-
30 logenetic model would help to identify who infected whom in instances in which this was
31 previously impossible. Using whole-genome sequences from SARS-CoV-2 multi-institutional
32 outbreaks as an example, we show how within-sample diversity is stable among repeated
33 serial samples from the same host, is transmitted between those cases with known epidemi-
34 ological links, and how this improves phylogenetic inference and our understanding of who
35 infected whom. Our technique is applicable to other infectious diseases and has immediate
36 clinical utility in infection prevention and control.

37 Introduction

38 Understanding who infects whom in an infectious disease outbreak is a key component of
39 infection prevention and control [1]. The use of whole-genome sequencing allows for detailed
40 investigation of disease outbreaks, but the limited genetic diversity of many pathogens often
41 hinders our understanding of transmission events [2]. As a consequence of the limited diver-
42 sity, many index case and contact pairs will share identical genotypes, making it difficult to
43 ascertain who infected whom.

44

45 Within-sample genetic diversity is common among a wide variety of pathogens [3–7].
46 This diversity may be generated *de novo* during infection, by a single transmission event of
47 a diverse inoculum or by independent transmission events from multiple sources [8]. The
48 maintenance and dynamic of within-host diversity is then a product of natural selection,
49 genetic drift, and fluctuating population size [1]. The transmission of within-host variation
50 between individuals is also favored as a large inoculum exposure is more likely to give rise to
51 infection [9–14].

52

53 Most genomic and phylogenetic workflows involve either genome assembly or alignment of
54 sequencing reads to a reference genome. In both cases, conventionally the resulting alignment
55 exclusively represents the most common nucleotide at each position. This is often referred
56 to as the consensus sequence. Although genome assemblers may output contigs (combined
57 overlapping reads) representing low frequency haplotypes, only the majority contig is kept
58 in the final sequence. In a mapping approach, a frequency threshold for the major variant
59 is usually pre-determined, under which a position is considered ambiguous. The lack of ge-
60 netic variation between temporally proximate samples and the slow mutation rate of many
61 pathogens results in direct transmission events sharing exact sequences between the hosts
62 when using the consensus sequence approach. For instance, the substitution rate of SARS-
63 CoV-2 has been inferred to be around 2 mutations per genome per month [15]. Given its
64 infectious period of 6 days [16], most consensus sequences in a small-scale outbreak will show
65 no variation between them. This lack of resolution and poor phylogenetic signal complicate
66 the determination of who infected whom, relying exclusively on epidemiological information.

67

68 We hypothesize that the failure of consensus sequence approaches to capture within-
69 sample variation arbitrarily excludes meaningful data and limits the ability to determine
70 who infected whom, and that including within-sample diversity in a phylogenetic model
71 would significantly increase the evolutionary and temporal signal and thereby improve our
72 ability to infer infectious diseases transmission events.

73

74 We tested our hypothesis on multi-institutional SARS-CoV-2 outbreaks across London
75 hospitals that were part of the COVID-19 Genomics UK (COG-UK) consortia [17]. Tech-
76 nical replicates, repeated longitudinal sampling from the same patient, and epidemiological
77 data allowed us to evaluate the presence and stability of within-sample diversity within the

78 host and in independently determined transmission chains. We also evaluated the use of
79 within-sample diversity in phylogenetic analysis by conducting simulations of sequencing
80 data using a phylogenetic model that accounts for the presence and transmission of within-
81 sample variation. We show the effects on phylogenetic inference of using consensus sequences
82 in the presence of within-sample diversity, and propose that existing phylogenetic models
83 can leverage the additional diversity given by the within-sample variation and reconstruct
84 the phylogenetic relationship between isolates. Lastly, we show that by taking into account
85 within-sample diversity in a phylogenetic model we improve the temporal signal in SARS-
86 CoV-2 outbreak analysis. Using both phylogenetic outbreak reconstruction and simulation
87 we show that our approach is superior to the current gold standard whole-genome consensus
88 sequence methods.

89 Results

90 Sampling, demographics and metadata

91 Between March 2020 and November 2020, 451 healthcare workers, patients and patient con-
92 tacts at the participating North London Hospitals were diagnosed at the Camelia Botnar
93 Laboratories with SARS-CoV-2 by PCR as part of a routine staff diagnostic service at Great
94 Ormond Street Hospital NHS Foundation Trust (GOSH). The mean participant age was 40
95 years old (median 38.5 years old, interquartile range (IQR) 30-50 years old), and 60% of
96 the participants were female (Supplementary Table 1). A total of 289 were whole-genome se-
97 quenced using the Illumina NextSeq platform, which resulted in 522 whole-genome sequences
98 including longitudinal and technical replicates (Supplementary Data File 1). All samples were
99 SARS-CoV-2 positive with real time qPCR cycle threshold (C_t) values ranging from 16 to
100 35 cycles (Supplementary Table 1). The earliest sample was collected on 26th March 2020,
101 while the latest one dated to 4th November 2020 (Supplementary Fig. 1a). A total of 291
102 samples had self-reported symptom onset data, for which the mean time from symptom onset
103 to sample collection date was 5 days (IQR 2-7 days, Supplementary Fig. 1b). More than 90%
104 of the samples were taken from hospital staff, while the rest comprised patients and contacts
105 of either the patients or the staff members (Supplementary Table 1).

106 Genomic analysis of SARS-CoV-2 sequences

107 Whole-genome sequences were mapped to the reference genome resulting in a mean coverage
108 depth of 2177x (Supplementary Fig. 2). A total of 454 whole-genomes with mean coverage
109 higher than 10x were kept for further analysis. Allele frequencies were extracted using the
110 pileup functionality within *bcftools* [18] with a minimum base and mapping quality of 30,
111 which represents a base call error rate of 0.1%. Variants were filtered further for read position
112 bias and strand bias. Only minor variants with an allele frequency of at least 1% were kept as
113 putative variants. Samples with a frequency of missing bases higher than 10% were excluded,
114 keeping 350 isolates for analysis. The mean number of low frequency variants was 12 (median
115 3, IQR 1.00 – 9.75), although both the number of variants and its deviation increased at high
116 C_t values (Supplementary Fig. 3).

117 Within-sample variation is stable between technical replicates

118 To understand the stability of within-sample variation and minimize spurious variant calls,
119 we sequenced and analyzed technical replicates of 17 samples. Overall, when the variant
120 was present in both duplicates the correlation of the variant frequencies was high ($R^2 = 0.9$,
121 Fig. 1a right). The high correlation was also maintained at low variant frequencies (Fig. 1a
122 left).

123
124 Minor variants were less likely to be detected or shared when one or more of the paired
125 samples had a low viral load. These discrepancies may appear because of amplification bias

126 caused by low genetic material, base calling errors due to low coverage, or low base quality.
127 The mean proportion of discrepant within-sample variants between duplicated samples was
128 0.39 (sd = 0.29), although this varied between duplicates (Supplementary Fig. 4). C_t values
129 in RT-PCR obtained during viral amplification are inversely correlated with low viral load
130 [19]. The proportion of shared intra-host variants was negatively correlated with C_t values
131 in a logistic model (estimate=-0.78, p-value=0.008), with higher C_t values associated with a
132 lower amount of shared intra-host variants (Fig. 1c). The number of within-sample variants
133 detected also increased with C_t value, as well as the deviation in the number of variants
134 between duplicates (Fig. 1d). This could be explained either by an increase in the number
135 of spurious variants at low viral loads [20], biased amplification of low level sub-populations
136 minor rare alleles [21], or due to the accumulation of within-host variation through time, as
137 viral load (with rising C_t values) also decreases from time since infection.

138
139 Based on these results, only samples with a C_t value equal or lower than 30 cycles were
140 considered, which resulted in 249 samples kept for analysis. For the filtered dataset, 414 out
141 of 29903 positions were polymorphic for the consensus sequence, while the alignment with
142 within-sample diversity had 1039 SNPs. Of these, 699 positions had intra-host diversity, of
143 which 78% (549/699) were singletons. The majority of samples (207/249, 83%) contained at
144 least 1 position with a high quality within-host variant, and the median amount of intra-host
145 variants per sample was 2 (IQR 1-4.5).

146 **Within-sample variation is shared between epidemiologically linked** 147 **samples**

148 Given the limited genomic information in the consensus sequences, epidemiological data is
149 often necessary to infer the directionality of transmission. We performed a pairwise compar-
150 ison of all samples and calculated the proportion of shared within-sample variants (shared
151 variants divided by total variants in the pair). We compared samples that a) did not have
152 any recorded epidemiological link, b) samples that were from the same hospital (possibly
153 linked), c) samples that were part of the same department within the same hospital (prob-
154 able link), and d) samples that had an epidemiological link within the same department of
155 the same hospital (proven link), e) were a longitudinal replicate from the same patient and
156 f) a technical replicate from the same sample.

157
158 We tested the concordance between epidemiological and genomic data by determining the
159 genetic distance between pairs of samples with epidemiological links and without them. Pairs
160 of samples from the same hospital, department, epidemiologically linked, or longitudinal and
161 technical replicates were more closely located in the consensus phylogenetic tree than those
162 samples that did not have any relationship, although this difference was small in the case of
163 pairs of samples from the same hospital (Table 1).

164
165 The proportion of shared within-host variants was significantly higher between technical

166 replicates, longitudinal duplicates, epidemiologically linked samples, and samples taken from
167 individuals from the same department when compared to pairs with no epidemiological links
168 (Fig. 2). The probability of sharing a low frequency variant was inferred using a logistic
169 regression model (Supplementary Fig. 5). There was a tendency for the probability to increase
170 with variant frequency, but the association was not strong (Odds ratio 1.8, 95% CI 0.9 – 3.5,
171 $p=0.08$). The probability of sharing a variant for samples with no epidemiological links was
172 9.5×10^{-6} (95% CI $8.8 \times 10^{-6} - 1.02 \times 10^{-5}$). Samples from the same hospital did not have a
173 probability significantly higher than those without any link (3.3×10^{-3} , 95% CI $2.7 \times 10^{-3} -$
174 4.03×10^{-3}). On the other hand, pairs from the same department, with epidemiological links,
175 replicates or technical replicates all had a higher probability of sharing a low frequency variant
176 when compared to those pairs with no link (all p -values < 0.001). The inferred probabilities
177 for pairs from the sample department was 1.4% (95% CI 0.9% – 2.1%), which increased to
178 5% for pairs with epidemiological links (95% CI 4.2% – 6.4%). For longitudinal replicates,
179 the probability was inferred to be 38% (95% CI 35% – 41%), while technical replicates were
180 estimated to have the highest probability (70%, 95% CI 64% – 76%).

181 **Within-host diversity model outperforms the consensus model in sim-** 182 **ulations**

183 The effect of within-sample diversity in phylogenetic inference was tested by evaluating the
184 accuracy in the reconstruction of known phylogenetic trees using a conventional phylogenetic
185 model and a model that accounts for within-sample variation.

186
187 The presence of within-sample diversity was coded in the genome alignment using exist-
188 ing IUPAC nomenclature [22]. For the consensus sequence alignment, only the 4 canonical
189 nucleotides were used (Fig. 3a,b), while the proposed alignment retained the major and mi-
190 nor allele information as independent character states (Fig. 3c,d).

191
192 In order to evaluate the bias in tree inference with and without the inclusion of within-
193 sample diversity, we simulated genome alignments for 100 random trees using a phylogenetic
194 model where both major and minor variant combinations were considered, resulting in a total
195 of 16 possible states (Fig. 3d) and the substitution rates shown in Supplementary Table 3.
196 From the simulated genomes, two types of alignments were generated: a consensus sequence,
197 where only the major allele was considered (Fig. 3a); and an alignment that retained the
198 major and minor allele information as independent character states (Fig. 3c). From the
199 simulated alignments, RaxML-NG was used to infer phylogenetic trees [23]. The consensus
200 sequence was analyzed with a GTR+ γ model, while the PROTGTR+ γ model was used in
201 order to accommodate the extra characters of the alignment with within-sample diversity
202 and major/minor variant information.

203
204 The two models were evaluated for their ability to infer the known phylogeny that in-
205 cluded within-host diversity. The estimated phylogenies were compared to the known tree

206 using different measures to capture dissimilarities in a variety of aspects relevant to tree
207 inference (Supplementary Table 2). For all the metrics employed, the phylogenies inferred
208 explicitly using within-host diversity as independent characters approximated better to the
209 initial tree than the one using the consensus sequence (Fig. 4). Additionally, the transi-
210 tion/transversion rates inferred by the phylogenetic models accounting for within-host diver-
211 sity accurately reflect the rates used for the simulation of genomic sequences (Supplementary
212 Table 3-5).

213 **Within-host diversity improves the resolution in SARS-CoV-2 phy-** 214 **logenetics**

215 Genome sequences collected at different time points are expected to diverge as time pro-
216 gresses, resulting in a positive correlation between the isolation date and the number of
217 accumulated mutations (temporal signal) [24]. The alignment with consensus sequences and
218 the one reflecting within-sample variation were used to infer two different phylogenetic trees
219 (Supplementary Fig. 6). Longitudinal samples in the phylogeny inferred using within-host
220 diversity reflected the expected temporal signal, with an increase in genetic distance as time
221 progressed between the longitudinal pairs in a linear model (coefficient 2.24, 0.59 - 3.88 95%
222 CI, $p = 0.019$, Supplementary Fig. 7). The difference in C_t value among longitudinal dupli-
223 cates was not correlated with a higher genetic distance (coefficient 1.62, -0.66 - 3.91 95% CI,
224 $p = 0.2$).

225
226 We analyzed the impact of using within-sample variation on the temporal structure of
227 the phylogeny by systematically identifying clusters of tips in the phylogenetic tree with an
228 identical consensus sequence and no temporal signal. We then performed a root-to-tip anal-
229 ysis using the tree inferred with intra-sample diversity. Only clusters with more than 3 tips
230 were used for the root-to-tip analysis. The majority of clusters (10/11) showed a positive cor-
231 relation between the distance of the tips to the root and the collection dates, demonstrating
232 a significant temporal signal between samples when there was none using the conventional
233 consensus tree (Fig. 5).

234
235 To illustrate the downstream application of the improved phylogenetic resolution, we in-
236 ferred a time-calibrated phylogeny with the collection dates of the tips using BactDating [25]
237 (Supplementary Fig. 8) and calculated the likelihood of transmission events within poten-
238 tial epidemiologically identified outbreaks using a Susceptible-Exposed-Infectious-Removed
239 (SEIR) model [26]. The SEIR model was parameterized with an average latency period of 5.5
240 days [27], an infectious period of 6 days [16], and a within-host coalescent rate of 5 days as
241 previously estimated for SARS-CoV-2 [28]. The likelihood of transmission was calculated for
242 every pair of samples, while the Edmonds algorithm as implemented in the R package *RBGL*
243 [29] was used to infer the graph with the optimum branching (Fig. 6c,d; Supplementary
244 Fig. 9).

245 Discussion

246 Detailed investigation of transmission events in an infectious disease outbreak is a prerequi-
247 site for effective prevention and control. Although whole-genome sequencing has transformed
248 the field of pathogen genomics, insufficient pathogen genetic diversity between cases in an
249 outbreak limits the ability to infer who infected whom. Using multi-hospital SARS-CoV-2
250 outbreaks and phylogenetic simulations, we show that including the genetic diversity of sub-
251 populations within a clinical sample improves phylogenetic reconstruction of SARS-CoV-2
252 outbreaks and determines the direction of transmission when using a consensus sequence
253 approach fails to do so.

254

255 The majority of samples sequenced harbored variants at low frequency that remained sta-
256 ble in technical replicates. However, within-host variation was less consistent between paired
257 samples with a lower viral load (higher C_t). This is likely to be a consequence of low starting
258 genetic material giving rise to amplification bias during library preparation and sequencing.
259 Establishing a cut-off for high C_t values is therefore important to accurately characterize
260 within-host variation. In our study, we excluded samples with a C_t value higher than 30
261 cycles based on the diagnostic PCR used at GOSH. Since C_t values are only a surrogate for
262 viral load and are not standardized across different assays [30], appropriate thresholds would
263 need to be determined for other primary PCR testing assays.

264

265 The generation, maintenance and evolution of subpopulations within the host reflect evo-
266 lutionary processes which are meaningful from phylogenetic and epidemiological perspectives.
267 Subpopulations within a host can emerge from three mechanisms: de novo diversification in
268 the host, transmission of a diverse inoculum, or multiple transmission events from different
269 sources. If the subpopulations are the result of de novo mutations, nucleotide polymorphisms
270 within the subpopulations accumulate over time and may therefore result in a phylogenetic
271 signal useful for phylogenetic inference. In our data, longitudinal samples taken at later
272 time points were demonstrated to accrue genomic variation. Although this pattern can be
273 confounded by decreasing viral load as infection progresses, C_t values in our dataset were not
274 correlated with a higher genetic distance, and clusters in our data containing both longitudi-
275 nal and technical replicates also corroborate these results. Transmission of a diverse inoculum
276 also gives rise to phylogenetically informative shared low frequency variants, as our results
277 show that immediate transmission pairs are more likely to share variants at low frequency.
278 The effect of multiple transmission events in the phylogeny depends on the relatedness of
279 both index cases and the bottleneck size in each transmission event.

280

281 Paired samples with epidemiological links and from the same department shared a higher
282 proportion of low frequency variants and were located closer in the consensus tree than sam-
283 ples with no relationship. Similarly, samples with shorter distance in the consensus phylogeny
284 were more likely to share low frequency variants. These patterns suggest that the distribution
285 of low frequency variants is linked to events of evolutionary and epidemiological interest. The

286 fact that technical duplicates shared more within-host diversity than longitudinal replicates
287 of the same sample suggests that much of the variation within hosts is transitory. There-
288 fore, within-host diversity may be relevant on relatively short time scales, which is precisely
289 where consensus sequences lack resolution. Combining the data derived from fixed alleles in
290 the consensus sequences and transient within-sample minor variation enables an improved
291 understanding of the relatedness of pathogen populations between hosts.

292

293 The effects of neglecting within-host diversity in phylogenetic inference were analyzed
294 by using simulated sequences under a phylogenetic model that reflects the presence and evo-
295 lution of within-host diversity. We compared a conventional consensus phylogenetic model
296 and a model that leverages within-sample diversity, and evaluated their ability to infer the
297 known phylogeny. Our proposed phylogenetic model incorporates within-sample variation by
298 explicitly coding major and minor nucleotides as independent characters in the alignment.
299 We demonstrated that phylogenies inferred using the conventional consensus sequence ap-
300 proach were heavily biased and unrepresentative of the known structure of the simulated
301 tree. However, sequences that included within-host diversity were shown to infer less biased
302 phylogenetic trees.

303

304 Previous studies have addressed the use of within-host variation to infer transmission
305 events. Wymant et al. [31] employed a framework based on phylogenetic inference and an-
306 cestral state reconstruction of each set of populations detected within read alignments using
307 genomic windows. Our study extends this work by coding genome-wide diversity within the
308 host directly in the alignment and the phylogenetic model. De Maio et al [32] proposed direct
309 inference of transmission from sequencing data alongside host exposure time and sampling
310 date within the bayesian framework BEAST2 [33]. Our approach is focused on directly im-
311 proving the temporal and phylogenetic signal of whole-genome sequences, and it's especially
312 suited for use in applications and analysis that employ a phylogenetic tree as input to infer
313 transmission [34].

314

315 Future work will extend this model by including allele frequency data in addition to
316 independent characters for major and minor variants. Phylogenetic models that explicitly
317 include dynamics of within-sample variation and sequencing error may further improve phy-
318 logenetic inference or allow researchers to better estimate parameters of interest, including
319 R_0 , bottleneck size, transmissibility and the origin of outbreaks.

320

321 Our study benefited from the availability of sequenced technical replicates that enabled us
322 to distinguish genuine variation from sequencing noise, especially at low variant frequencies.
323 Similarly, access to longitudinal samples from the same patient allowed us to characterize the
324 spectrum of within host variation and therefore reconstruct transmission chains with more
325 precision.

326

327 In line with conventional consensus sequencing approaches, we used a reference sequence

328 for genome alignment and variant calling. Although widely used, one limitation of this ap-
329 proach is a potential mapping bias causing some reads to reflect the reference base at low
330 frequencies at a position where only a variant should be present. Although we applied strin-
331 gent quality filtering, we cannot rule out the persistence of some false positive minor variants.
332 Using genome graphs to map to a reference that encompasses a wider spectrum of variation
333 may alleviate this problem, and could be an interesting addition to pathogen population
334 genomic analysis.

335

336 Our results demonstrate that within-sample variation can be leveraged to increase the
337 resolution of phylogenetic trees and improve our understanding of who infected whom. Using
338 SARS-CoV-2 as an example, we show that variants at low frequencies are stable, phyloge-
339 netically informative and are more often shared among epidemiologically related contacts.
340 We propose that pathogen phylogenetic models should accommodate within-host variation
341 to improve the understanding of infectious disease transmission.

342 **Materials and methods**

343 **Model for within-host diversity**

344 Whole-genome alignments were generated from 100 random phylogenetic trees with 100 tips
345 with the function *SimSeq* of the R package *phangorn* [35, 36] using a model with 16 char-
346 acter states that represent the combinations of the 4 nucleotides with each other as minor
347 and major alleles (Fig. 3d). Three substitution rates for the model were considered: a rate
348 at which minor variants evolve, equal to 1; the rate at which minor variants are lost, leaving
349 only the major nucleotide at that position, equal to 100; and the rate at which minor/major
350 variants are switched, equal to 200.

351

352 Two types of alignments were generated from the simulated genomes: a consensus se-
353 quence, where only the major allele was considered; and an alignment that retained the
354 major and minor allele information as independent character states. RaxML-NG [23] was
355 used to infer phylogenetic trees. The consensus sequence was analyzed with a GTR+ γ model,
356 while the PROTGTR+ γ model was used for the alignment with intra-host diversity and ma-
357 jor/minor variant information.

358

359 Several metrics were used to compare the 200 inferred phylogenetic trees with their respec-
360 tive starting phylogeny from which the sequences were simulated (Supplementary Table 2).
361 We chose metrics available in R suitable for unrooted trees, using the option ‘rooted=FALSE’
362 where appropriate. The Robinson-Foulds (RF) distance [37] calculates the number of splits
363 differing between both phylogenetic trees. For the weighted Robinson-Foulds (wRF), the
364 distance is expressed in terms of the branch lengths of the differing splits. The Kuhner-
365 Felsenstein distance [38] considers the edge length differences in all splits, regardless of
366 whether the topology is shared or not. Last, the Penny-Steel distance or path difference
367 metric [39] calculates the pairwise differences in the path of each pair of tips, with the
368 weighted Penny-Steel distance (wPS) using branch length to compute the path differences.
369 All functions were used as implemented in the package *phangorn* [36] within R [35].

370 **Amplification and whole-genome sequencing**

371 SARS-CoV-2 real-time qPCR confirmed isolates from London hospitals were collected as part
372 of the routine diagnostic service at Great Ormond Street Hospital NHS Foundation Trust
373 (GOSH) [40] and the COVID-19 Genomics UK Consortium (COG-UK) [17] between March
374 and December 2020, in addition to epidemiological and patient metadata (Supplementary
375 Table 1). SARS-CoV-2 whole-genome sequencing was performed by UCL Genomics. cDNA
376 and multiplex PCR reactions were prepared following the ARTIC nCoV-2019 sequencing
377 protocol [41]. The ARTIC V3 primer scheme [42] was used for the multiplex PCR, with a
378 65°C, 5 min annealing/extension temperature. Pools 1 and 2 multiplex PCRs were run for 35
379 cycles. 5 μ L of each PCR were combined and 20 μ L nuclease-free water added. Libraries were

380 prepared on the Agilent Bravo NGS workstation option B using Illumina DNA prep (Cat.
381 20018705) with unique dual indexes (Cat. 20027213/14/15/16). Equal volumes of the final
382 libraries were pooled, bead purified and sequenced on the Illumina NextSeq 500 platform
383 using a Mid Output 150 cycle flowcell (Cat. 20024904) (2 x 75bp paired ends) at a final
384 loading concentration of 1.1pM.

385 **Whole-genome sequence analysis of SARS-CoV-2 sequences**

386 Raw illumina reads were quality trimmed using Trimmomatic [43] with a minimum mean
387 quality per base of 20 in a 4-base wide sliding window. The 5 leading and trailing bases of each
388 read were removed, and reads with an average quality lower than 20 were discarded. The re-
389 sulting reads were aligned against the Wuhan-Hu-1 reference genome (GenBank NC_45512.2,
390 GISAID EPI_ISL_402125) using BWA-mem v0.7.17 with default parameters [44]. The
391 alignments were subsequently sorted by position using SAMtools v1.14 [45]. Primer se-
392 quences were masked using ivar [46].

393

394 Single-nucleotide variants were identified using the pileup functionality of samtools [45]
395 via the pysam package in Python (<https://github.com/pysam-developers/pysam>). Vari-
396 ants were further filtered using bcftools [18]. Only variants with a minimum depth of 50x
397 and a minimum base quality and mapping quality of 30 were kept. Additionally, variants
398 within low complexity regions identified by sdust (<https://github.com/lh3/sdust>) were re-
399 moved. For positions where only one base was present, the minimum depth was 20 reads,
400 with at least 5 reads in each direction. Positions with low frequency variants were filtered if
401 the total coverage at that position was less than 100x, with at least 20 reads in total and 5
402 reads in each strand supporting each of the main two alleles.

403

404 Two different alignments were prepared from the data. First, an alignment of the con-
405 sensus sequence where the most prevalent base at each position was kept. Variants where
406 the most prevalent allele was not supported by more than 60% of the reads were considered
407 ambiguous. Additionally, an alignment reflecting within-sample variation at each position as
408 well as which base is the most prevalent and which one appears at a lower frequency by using
409 the IUPAC nomenclature for amino acids [22].

410

411 For the two different alignments, maximum likelihood phylogenies were inferred by us-
412 ing RAxML-NG [23] with 20 starting trees (10 random and 10 parsimony), 100 bootstrap
413 replicates, and a minimum branch length of 10^{-9} . For the consensus sequence, the GTR
414 model was used. For the alignment reflecting within-host diversity, a model with amino acid
415 nomenclature (PROTGTR) was used. All models allowed for a γ distributed rate of variation
416 among sites.

417 **Data availability**

418 Samples sequenced as part of this study have been submitted to the European Nucleotide
419 Archive under accession PRJEB53224. Sample metadata is included in Supplementary Data
420 File 1.

421 **Code availability**

422 All custom code used in this article can be accessed at
423 https://github.com/arturotorres/scov2_withinHost.git.

424 References

- 425 1. Didelot, X., Bowden, R., Wilson, D. J., Peto, T. E. & Crook, D. W. Transforming clinical microbiology
426 with bacterial genome sequencing. *Nature Reviews Genetics* (2012).
- 427 2. Campbell, F., Strang, C., Ferguson, N., Cori, A. & Jombart, T. When are pathogen genome sequences
428 informative of transmission events? *PLoS Pathogens* (2018).
- 429 3. Mongkolrattanothai, K. *et al.* Simultaneous carriage of multiple genotypes of *Staphylococcus aureus* in
430 children. *Journal of medical microbiology* **60**, 317–322 (2011).
- 431 4. Lieberman, T. D. *et al.* Genomic diversity in autopsy samples reveals within-host dissemination of
432 HIV-associated *Mycobacterium tuberculosis*. *Nature medicine* **22**, 1470–1474 (2016).
- 433 5. Dinis, J. M. *et al.* Deep Sequencing Reveals Potential Antigenic Variants at Low Frequencies in Influenza
434 A Virus-Infected Humans. *Journal of Virology* **90**, 3355–3365 (2016).
- 435 6. Leitner, T. Phylogenetics in HIV transmission: Taking within-host diversity into account. *Current Opin-*
436 *ion in HIV and AIDS* **14**, 181–187 (2019).
- 437 7. Popa, A. *et al.* Genomic epidemiology of superspreading events in Austria reveals mutational dynamics
438 and transmission properties of SARS-CoV-2. *Science Translational Medicine* **12**, 2555 (2020).
- 439 8. Worby, C. J., Lipsitch, M. & Hanage, W. P. Within-Host Bacterial Diversity Hinders Accurate Recon-
440 struction of Transmission Networks from Genomic Distance Data. *PLoS Computational Biology* (2014).
- 441 9. Murphy, B. R. *et al.* Dose Response of Cold-Adapted, Reassortant Influenza A/California/10/78 Virus
442 (H1N1) in Adult Volunteers. *Journal of Infectious Diseases* **149**, 816–816 (1984).
- 443 10. Han, A. *et al.* A Dose-finding Study of a Wild-type Influenza A(H3N2) Virus in a Healthy Volunteer
444 Human Challenge Model. *Clinical Infectious Diseases* **69**, 2082–2090 (2019).
- 445 11. Lee, L. Y. W. *et al.* Severe Acute Respiratory Syndrome Coronavirus 2 (SARS-CoV-2) Infectivity by
446 Viral Load, S Gene Variants and Demographic Factors, and the Utility of Lateral Flow Devices to
447 Prevent Transmission. *Clinical Infectious Diseases* (2021).
- 448 12. Sender, R. *et al.* The total number and mass of SARS-CoV-2 virions. *Proceedings of the National*
449 *Academy of Sciences of the United States of America* **118** (2021).
- 450 13. Spinelli, M. A. *et al.* Importance of non-pharmaceutical interventions in lowering the viral inoculum to
451 reduce susceptibility to infection by SARS-CoV-2 and potentially disease severity. *The Lancet Infectious*
452 *Diseases* **21**, e296–e301 (2021).
- 453 14. Trunfio, M., Calcagno, A., Bonora, S. & Di Perri, G. Lowering SARS-CoV-2 viral load might affect
454 transmission but not disease severity in secondary cases. *The Lancet Infectious Diseases* **21**, 914–915
455 (2021).
- 456 15. Harvey, W. T. *et al.* SARS-CoV-2 variants, spike mutations and immune escape. *Nature Reviews Mi-*
457 *crobiology* **19**, 409–424 (2021).
- 458 16. Byrne, A. W. *et al.* Inferred duration of infectious period of SARS-CoV-2: rapid scoping review and
459 analysis of available evidence for asymptomatic and symptomatic COVID-19 cases. *BMJ open* **10**,
460 e039856 (2020).
- 461 17. COVID-19 Genomics UK (COG-UK). An integrated national scale SARS-CoV-2 genomic surveillance
462 network. *The Lancet. Microbe* **1**, e99–e100 (2020).
- 463 18. Danecek, P. *et al.* The variant call format and VCFtools. *Bioinformatics* **27**, 2156–2158 (2011).
- 464 19. Tom, M. R. & Mina, M. J. To Interpret the SARS-CoV-2 Test, Consider the Cycle Threshold Value.
465 *Clinical Infectious Diseases* **71**, 2252–2254 (2020).

- 466 20. Tonkin-Hill, G. *et al.* Patterns of within-host genetic diversity in SARS-CoV-2. *eLife* **10** (2021).
- 467 21. McCrone, J. T. & Lauring, A. S. Measurements of Intrahost Viral Diversity Are Extremely Sensitive
468 to Systematic Errors in Variant Calling. *Journal of Virology* **90**, 6884–6895 (2016).
- 469 22. IUPAC-IUB Joint Commission on Biochemical Nomenclature (JCBN). Nomenclature and symbolism
470 for amino acids and peptides. Recommendations 1983. *European journal of biochemistry* **138**, 9–37
471 (1984).
- 472 23. Kozlov, A. M., Darriba, D., Flouri, T., Morel, B. & Stamatakis, A. RAxML-NG: A fast, scalable and
473 user-friendly tool for maximum likelihood phylogenetic inference. *Bioinformatics* **35**, 4453–4455 (2019).
- 474 24. Rieux, A. & Balloux, F. Inferences from tip-calibrated phylogenies: a review and a practical guide.
475 *Molecular Ecology* **25**, 1911–1924 (2016).
- 476 25. Didelot, X., Croucher, N. J., Bentley, S. D., Harris, S. R. & Wilson, D. J. Bayesian inference of ancestral
477 dates on bacterial phylogenetic trees. *Nucleic Acids Research* **46**, e134–e134 (2018).
- 478 26. Eldholm, V. *et al.* Impact of HIV co-infection on the evolution and transmission of multidrug-resistant
479 tuberculosis. *eLife* **5** (2016).
- 480 27. Xin, H. *et al.* Estimating the Latent Period of Coronavirus Disease 2019 (COVID-19). *Clinical Infectious
481 Diseases* (2021).
- 482 28. Wang, L. *et al.* Inference of person-to-person transmission of COVID-19 reveals hidden super-spreading
483 events during the early outbreak phase. *Nature communications* **11**, 5006 (2020).
- 484 29. Carey, V., Long, L. & Gentleman, R. *RBGL: An interface to the BOOST graph library* 2021.
- 485 30. Evans, D. *et al.* The Dangers of Using Cq to Quantify Nucleic Acid in Biological Samples: A Lesson
486 From COVID-19. *Clinical chemistry* **68**, 153–162 (2021).
- 487 31. Wymant, C. *et al.* PHYLOSCANNER: Inferring transmission from within- and between-host pathogen
488 genetic diversity. *Molecular Biology and Evolution* (2018).
- 489 32. De Maio, N., Worby, C. J., Wilson, D. J. & Stoesser, N. Bayesian reconstruction of transmission within
490 outbreaks using genomic variants. *PLoS Computational Biology* (2018).
- 491 33. Bouckaert, R. *et al.* BEAST 2: A Software Platform for Bayesian Evolutionary Analysis. *PLoS Com-
492 putational Biology* (2014).
- 493 34. Didelot, X., Fraser, C., Gardy, J., Colijn, C. & Malik, H. Genomic infectious disease epidemiology in
494 partially sampled and ongoing outbreaks. *Molecular Biology and Evolution* (2017).
- 495 35. R Core Team & R Foundation for Statistical Computing. *R: A Language and Environment for Statistical
496 Computing* 2021.
- 497 36. Schliep, K. P. phangorn: phylogenetic analysis in R. *Bioinformatics* **27**, 592–593 (2011).
- 498 37. Robinson, D. & Foulds, L. Comparison of phylogenetic trees. *Mathematical Biosciences* **53**, 131–147
499 (1981).
- 500 38. Kuhner, M. K. & Felsenstein, J. A simulation comparison of phylogeny algorithms under equal and
501 unequal evolutionary rates. *Molecular Biology and Evolution* **11**, 459–468 (1994).
- 502 39. Steel, M. A. & Penny, D. Distributions of Tree Comparison Metrics-Some New Results. *Systematic
503 Biology* **42**, 126 (1993).
- 504 40. Storey, N. *et al.* Single base mutations in the nucleocapsid gene of SARS-CoV-2 affects amplification
505 efficiency of sequence variants and may lead to assay failure. *Journal of Clinical Virology Plus* **1**, 100037
506 (2021).
- 507 41. Tyson, J. R. *et al.* Improvements to the ARTIC multiplex PCR method for SARS-CoV-2 genome
508 sequencing using nanopore. *bioRxiv : the preprint server for biology* **3**, 2020.09.04.283077 (2020).

- 509 42. ARTIC Network. *ARTIC nanopore protocol for nCoV2019 novel coronavirus [Internet]*
- 510 43. Bolger, A. M., Lohse, M. & Usadel, B. Trimmomatic: a flexible trimmer for Illumina sequence data.
511 *Bioinformatics* **30**, 2114–2120 (2014).
- 512 44. Li, H. & Durbin, R. Fast and accurate long-read alignment with Burrows–Wheeler transform. *Bioin-*
513 *formatics* **26**, 589–595 (2010).
- 514 45. Li, H. *et al.* The Sequence Alignment/Map format and SAMtools. *Bioinformatics* **25**, 2078–2079 (2009).
- 515 46. Grubaugh, N. D. *et al.* An amplicon-based sequencing framework for accurately measuring intrahost
516 virus diversity using PrimalSeq and iVar. *Genome Biology* (2019).

517 **Acknowledgements**

518 The authors dedicate this article to the hospital staff members and patients who died of
519 coronavirus disease 2019. They also thank all staff and patients who have taken part in
520 the study. In addition, the authors are very grateful to the Great Ormond Street laboratory
521 staff, the staff at the Camelia Botnar Laboratory, the Great Ormond Street Institute of Child
522 Health and the COVID-19 sequencing team at UCLG who worked tirelessly to ensure that
523 all polymerase chain reaction tests and sequencing work were completed in a timely manner
524 during the COVID-19 pandemic. All authors acknowledge UCL Computer Science Technical
525 Support Group (TSG) and the UCL Department of Computer Science High Performance
526 Computing Cluster. LG was supported by the Wellcome Trust (201470/Z/16/Z), the Na-
527 tional Institute of Allergy and Infectious Diseases of the National Institutes of Health under
528 award number 1R01AI146338 and by the GOSH/ICH Biomedical Research Centre. XD was
529 supported by the NIHR Health Protection Research Unit in Genomics and Enabling Data.

530 **Author Contributions**

531 ATO, LG, XD, and MK conceived and designed the study. LG, NS, SR, RW, KH, CW and JB
532 performed and advised on sample preparation and whole-genome sequencing work. JH and
533 HD collected and analyzed epidemiological data. ATO, MK, XD, RG, JB and LG performed
534 and advised on statistical and computational analyses. ATO and LG wrote the manuscript
535 with input from all co-authors. All authors read and approved the final manuscript.

536 **Competing interests**

537 The authors declare no competing interests

538 **Ethics declarations**

539 Ethical approval was obtained for all individual studies from which this data was derived.

540 Tables

Table 1: Phylogenetic distance (substitutions per genome per year) between pairs of samples.

Sample relationship	Estimate (95%CI)	p-value
None	11.73 (11.63 - 11.83)	Reference
Hospital	10.3 (10.09 - 10.54)	$<1 \times 10^{-4}$
Department	5.35 (4.21 - 6.49)	$<1 \times 10^{-4}$
Epidemiological	1.62 (0.53 - 2.72)	$<1 \times 10^{-4}$
Longitudinal duplicates	0.01 (-1.84 - 1.86)	$<1 \times 10^{-4}$
Technical replicate	0 (-4.29 - 4.29)	$<1 \times 10^{-4}$

541 **Figures**

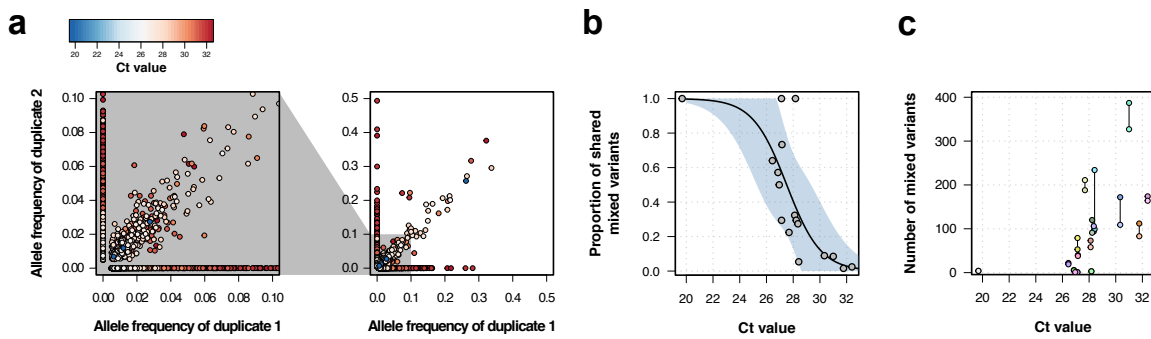


Figure 1: Genomic analysis of technical duplicates.

a Allele frequency comparison between technical replicates for all frequencies (right) and for frequencies up to 1% (left). Colors represent the C_t value for the sample. **b** Proportion of shared mixed variants between technical replicates in relation to the C_t value. **c** Total number of mixed variants in relation to the C_t value. Lines linked two technical replicates. Each sequence has a different color, with sequences from the same patient having a different shade of the same color.

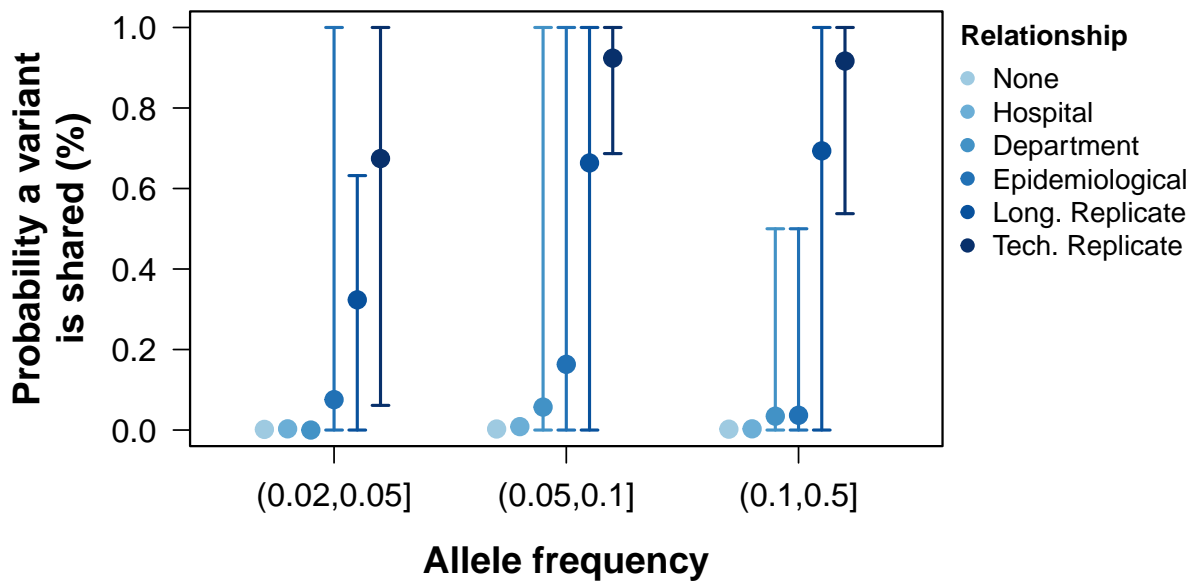


Figure 2: Probability of sharing within-host variants in sample pairs.

The probability of variants shared between pairs of samples calculated as the number of low frequency variants in both samples divided by the total number of variants between the pair. Colors grouped samples by their relationship. Points represent the mean probability a variant is shared between all pairwise samples within a group and allele frequency. Error bars show the 95% CI.

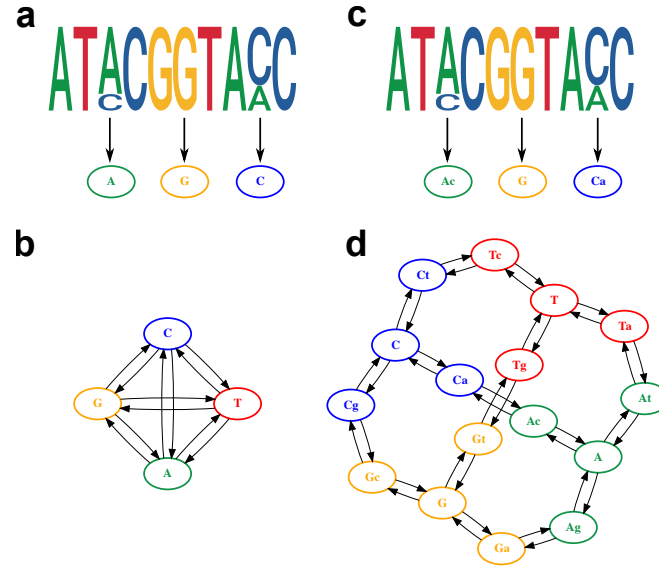


Figure 3: Model of within-host diversity.

Proposed evolutionary model of within-host diversity in genomic sequences. Upper-case letters represent the major variant in the population, while lowercase letters indicate presence of a minor variant alongside the major one. **a, c** Genome sequences where some positions show within-sample variation (top), represented by a major allele (big size letter) and a minor one (smaller size), as well as its representation in the alignment (bottom). **b, d** Models of nucleotide evolution. Character transitions are indicated by arrows. **a** Consensus sequence, where only the major allele is represented in the alignment. **b** Model of nucleotide evolution using the consensus sequence, with four character states representing the four nucleotides. **c** Sequence with within-sample variation, represented by an uppercase letter for the major allele and a lower case letter for the minor allele. **d** Model of nucleotide evolution with 16 character states accounting for within-sample variation.

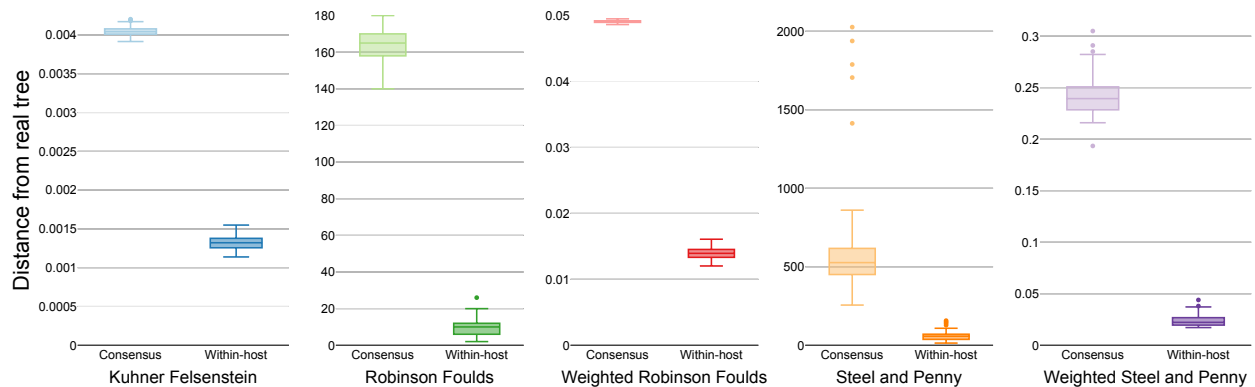


Figure 4: Similarity scores for inferred trees.

Comparison of the phylogenetic trees inferred using three simulated sequences and different phylogenetic models with the known starting tree. Colors differentiate the metrics used for the comparison.

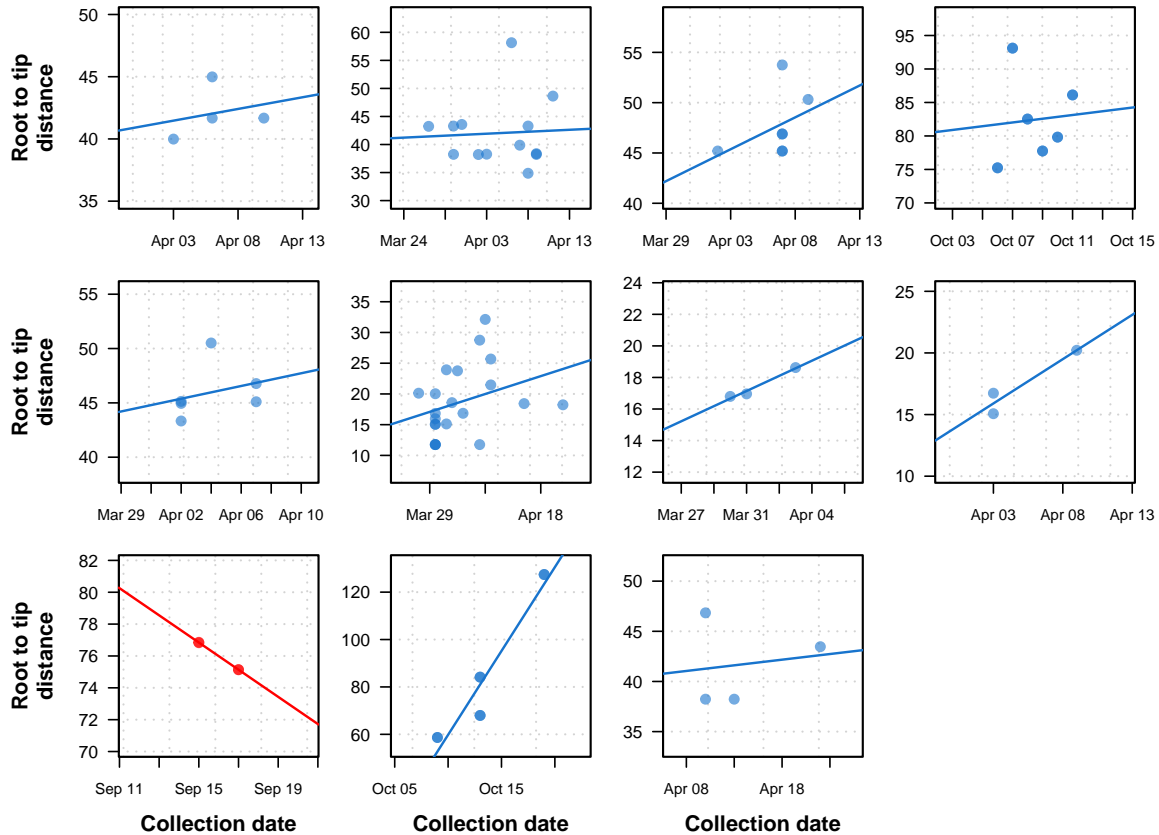


Figure 5: Previously uninformative clusters present temporal signal when using within-sample diversity.

A set of 11 outbreak clusters (one per panel, each plotting the root to tip distance against time) in which all samples had identical consensus genomes sequences (and therefore no temporal signal). Blue colors indicate those regressions that after utilizing within sample diversity now have a positive slope (temporal signal), and red shows those regressions that have a negative slope (misleading or false positive temporal signal).

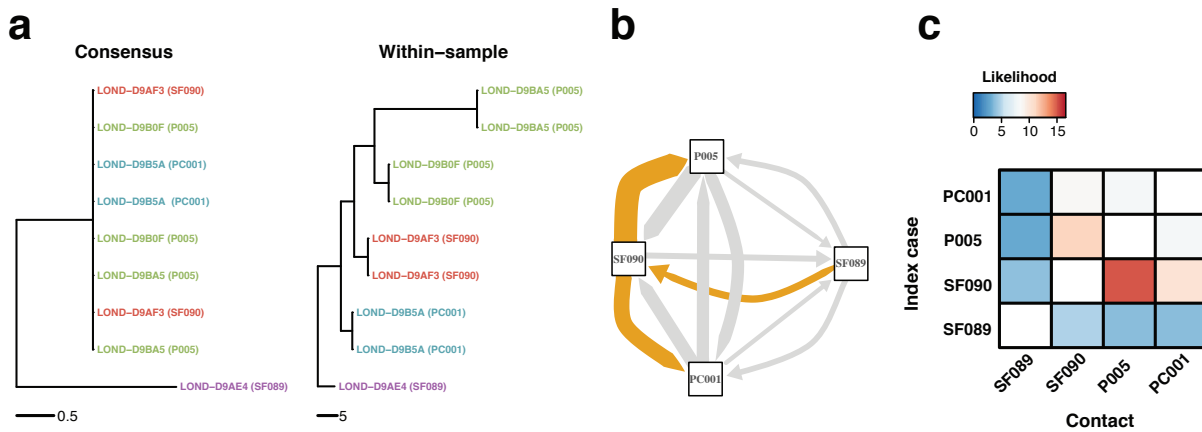


Figure 6: Within-sample variation improves resolution of infectious disease outbreaks.

Effect of using low frequency variants in phylogenetic inference. **a** Maximum likelihood phylogeny using the consensus sequences (left) and the alignment leveraging within-sample variation. Replicates of the same sample share the same color. Sample IDs are coded as follows: SF, for staff members; P, for patients; and PC, for patient contacts. **b** Transmission network inferred using within sample variation. Edge width is proportional to the likelihood of direct transmission using a Susceptible-Exposed-Infectious-Removed (SEIR) model. Colored edges represent the Edmunds optimum branching and thus the most likely chain. **c** Heatmap of the likelihood of direct transmission between all pairwise pairs of samples using a SEIR model. Vertical axis is the infector while the horizontal axis shows the infectee.

542 **Supplementary Information**

Supplementary Table 1: Sample collection and demographics.

	Number	Percentage
Total samples	451	100
Hospital		
Barnet, Enfield & Haringey Mental Health	18	3.99
Camden and Islington Mental Health	3	0.67
Chase Farm	1	0.22
FLARE Trial	3	0.67
GOSH	182	40.35
North Middlesex University Hospital	105	23.28
Royal Free Hospital	50	11.09
UCLH	10	2.22
Whittington Health	79	17.52
Missing	0	0
Role		
Staff	403	89.36
Patient	14	3.1
Contact	32	7.1
Missing	2	0.44
Sex		
Female	274	60.75
Male	161	35.7
Undertermined	3	0.67
Missing	13	2.88
Age		
(0,10]	8	1.77
(10,20]	9	2
(20,30]	111	24.61
(30,40]	111	24.61
(40,50]	98	21.73
(50,60]	74	16.41
(60,70]	22	4.88
(70,80]	10	2.22
(80,90]	3	0.67
Missing	5	1.11
Ct		
(15,20]	15	3.33
(20,25]	85	18.85
(25,30]	149	33.04
(30,35]	197	43.68
Missing	5	1.11

Supplementary Table 2: Metrics used for phylogenetic tree comparison.

Abbreviation	Name	Rooted trees	Branch length	R function & package
KF	Kuhner and Felsenstein	No	Yes	KF.dist, phangorn
RF	Robinson Foulds	No	No	RF.dist, phangorn
wRF	Weighted Robinson Foulds	No	Yes	wRF.dist, phangorn
PS	Penny and Steel path	No	No	path.dist, phangorn
wPS	Penny and Steel path	No	Yes	path.dist, phangorn

Supplementary Table 3: Transition/transversion rates and base frequencies of the known simulated tree.

	A	Ag	Ca	Ga	C	Ta	Gc	G	Tc	Tg	Gt	Ac	Cg	T	At	Ct	Base freqs.
A	-	-	-	-	-	-	-	-	-	-	-	-	-	-	-	-	0.22
Ag	20	-	-	-	-	-	-	-	-	-	-	-	-	-	-	-	0.01
Ca	0	0	-	-	-	-	-	-	-	-	-	-	-	-	-	-	0.01
Ga	0	200	0	-	-	-	-	-	-	-	-	-	-	-	-	-	0.01
C	0	0	1	0	-	-	-	-	-	-	-	-	-	-	-	-	0.22
Ta	0	0	0	0	0	-	-	-	-	-	-	-	-	-	-	-	0.01
Gc	0	0	0	0	0	0	-	-	-	-	-	-	-	-	-	-	0.01
G	0	0	0	1	0	0	1	-	-	-	-	-	-	-	-	-	0.22
Tc	0	0	0	0	0	0	0	0	-	-	-	-	-	-	-	-	0.01
Tg	0	0	0	0	0	0	0	0	0	-	-	-	-	-	-	-	0.01
Gt	0	0	0	0	0	0	0	20	0	200	-	-	-	-	-	-	0.01
Ac	20	0	200	0	0	0	0	0	0	0	0	-	-	-	-	-	0.01
Cg	0	0	0	0	20	0	200	0	0	0	0	0	-	-	-	-	0.01
T	0	0	0	0	0	1	0	0	1	1	0	0	0	-	-	-	0.22
At	20	0	0	0	0	200	0	0	0	0	0	0	0	0	-	-	0.01
Ct	0	0	0	0	20	0	0	0	200	0	0	0	0	0	0	-	0.01

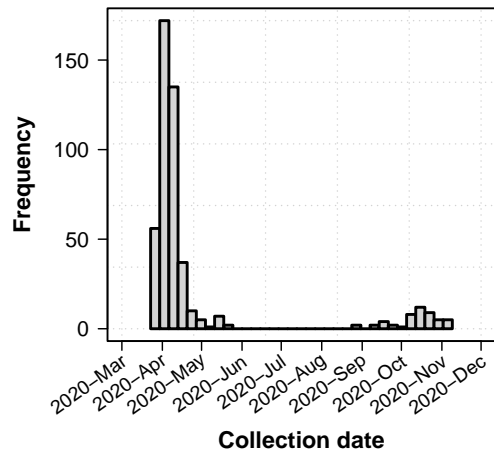
Supplementary Table 4: Inferred transition/transversion rates and base frequencies when using the consensus sequence. Numbers show the average of 100 simulations.

	A	C	G	T	Base freqs
A	-	-	-	-	0.255
C	0.974	-	-	-	0.250
G	1.088	1.148	-	-	0.247
T	0.854	0.996	1	-	0.248

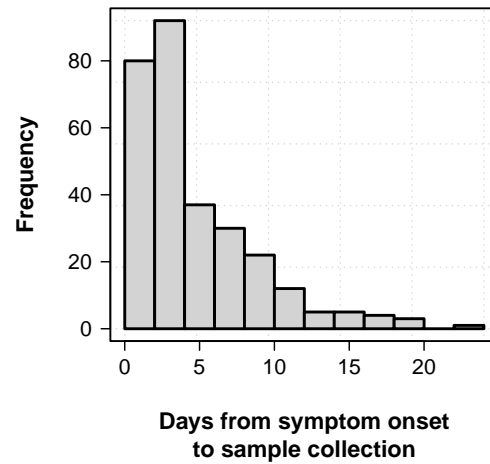
Supplementary Table 5: Inferred transition/transversion rates and base frequencies when accounting for within-host diversity. Numbers show the average of 100 simulations

	A	Ag	Ca	Ga	C	Ta	Gc	G	Tc	Tg	Gt	Ac	Cg	T	At	Ct	Base freqs.
A	-	-	-	-	-	-	-	-	-	-	-	-	-	-	-	-	0.22
Ag	17.35	-	-	-	-	-	-	-	-	-	-	-	-	-	-	-	0.01
Ca	0	0	-	-	-	-	-	-	-	-	-	-	-	-	-	-	0.01
Ga	0	185.96	0	-	-	-	-	-	-	-	-	-	-	-	-	-	0.01
C	0	0	1.86	0	-	-	-	-	-	-	-	-	-	-	-	-	0.22
Ta	0	0	0	0	0	-	-	-	-	-	-	-	-	-	-	-	0.01
Gc	0	0	0	0	0	0	-	-	-	-	-	-	-	-	-	-	0.01
G	0	0	0	1.16	0	0	1.08	-	-	-	-	-	-	-	-	-	0.21
Tc	0	0	0	0	0	0	0	0	-	-	-	-	-	-	-	-	0.01
Tg	0	0	0	0	0	0	0	0	0	-	-	-	-	-	-	-	0.01
Gt	0	0	0	0	0	0	0	21.64	0	196.56	-	-	-	-	-	-	0.01
Ac	16.51	0	183.53	0	0	0	0	0	0	0	0	-	-	-	-	-	0.01
Cg	0	0	0	0	21.20	0	200	0	0	0	0	0	-	-	-	-	0.01
T	0	0	0	0	0	0.98	0	0	1.05	1.26	0	0	0	-	-	-	0.21
At	17.70	0	0	0	0	175.58	0	0	0	0	0	0	0	0	-	-	0.01
Ct	0	0	0	0	20.09	0	0	0	188.86	0	0	0	0	0	0	-	0.01

a

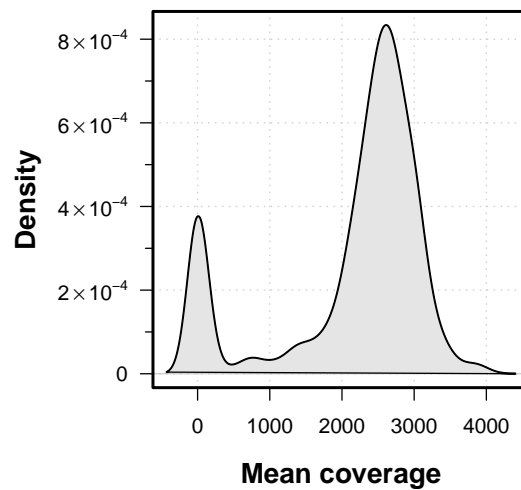


b



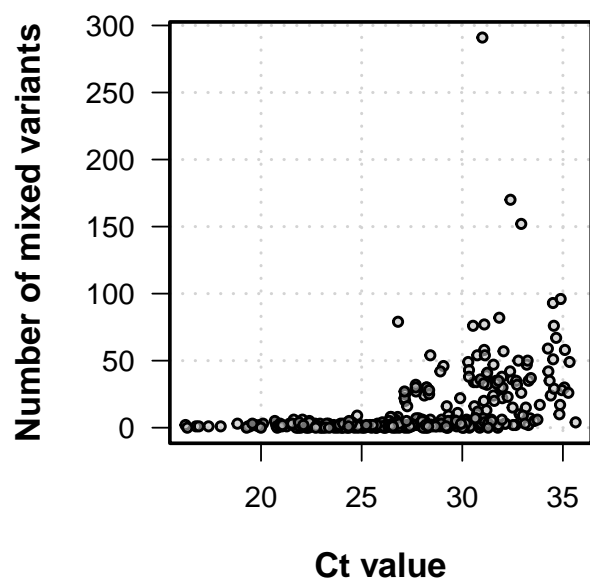
Supplementary Figure 1: Collection date distribution and time from symptom and days from symptom onset.

(a) Distribution of collection dates. (b) Histogram of time from symptom onset to sample collection.



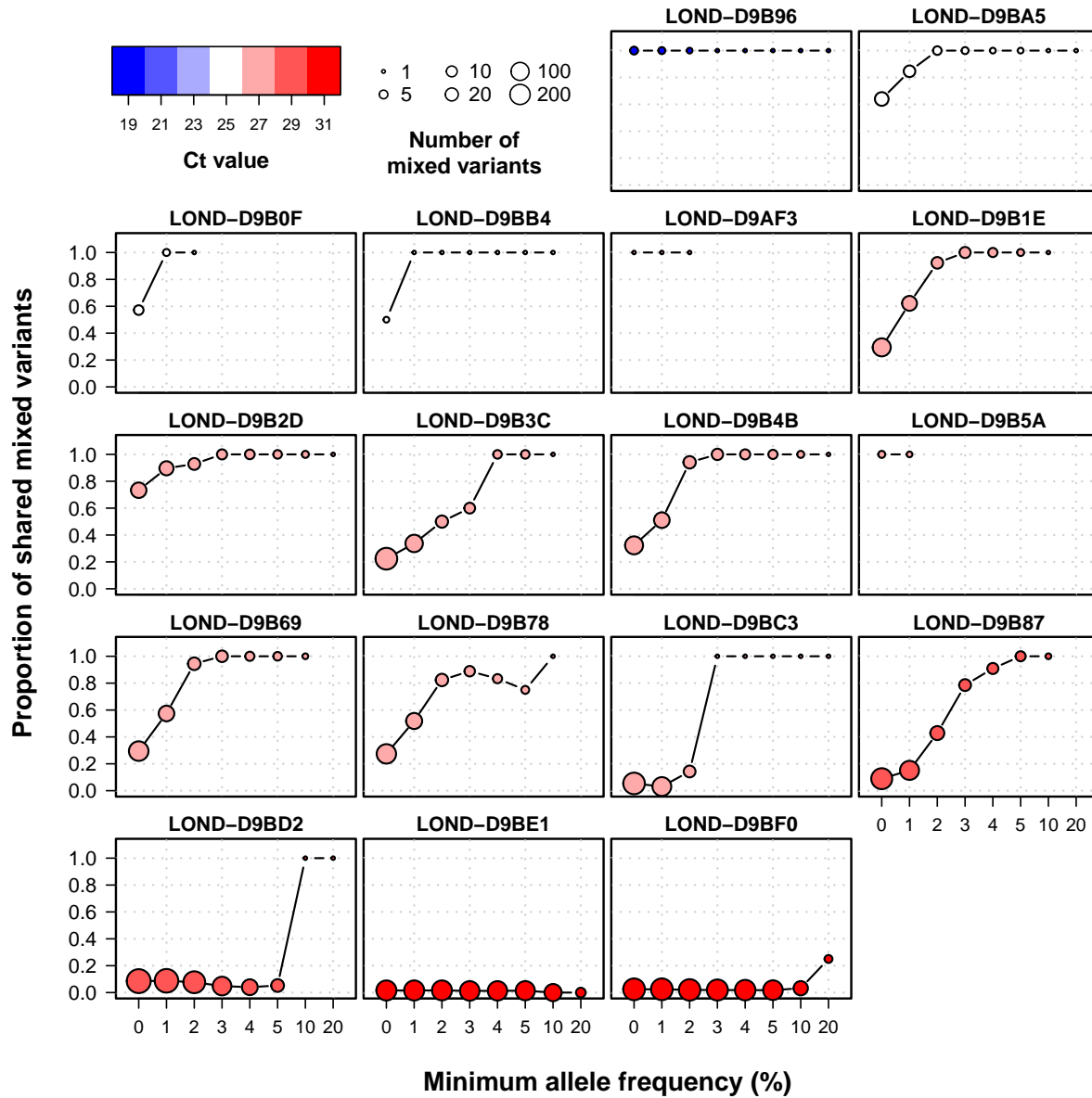
Supplementary Figure 2: Sample mean coverage distribution.

Density distribution of mean coverage.



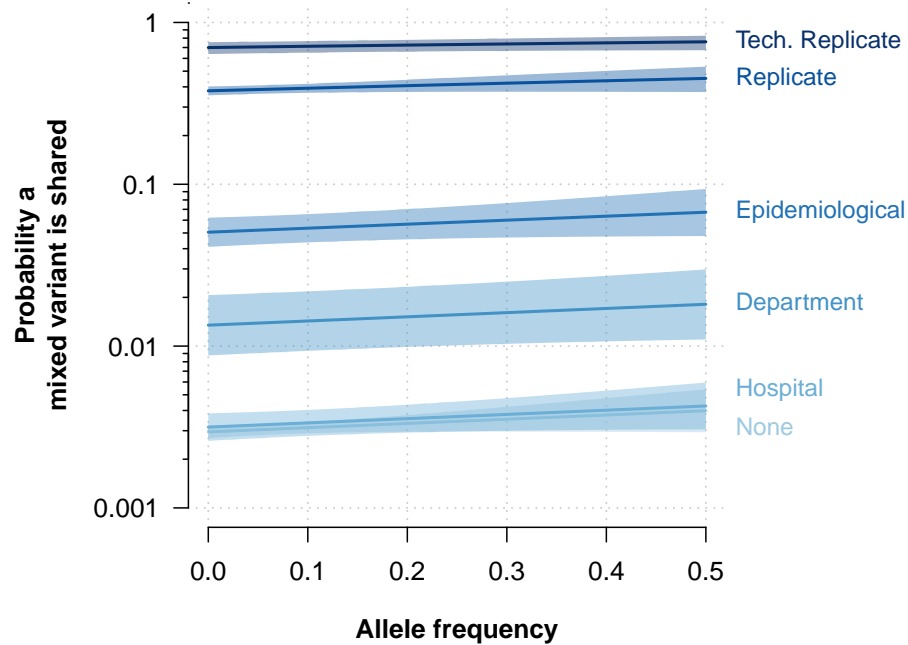
Supplementary Figure 3: Number of low frequency variants and C_t value.

Higher C_t values were linked to a higher number of within-sample variation.



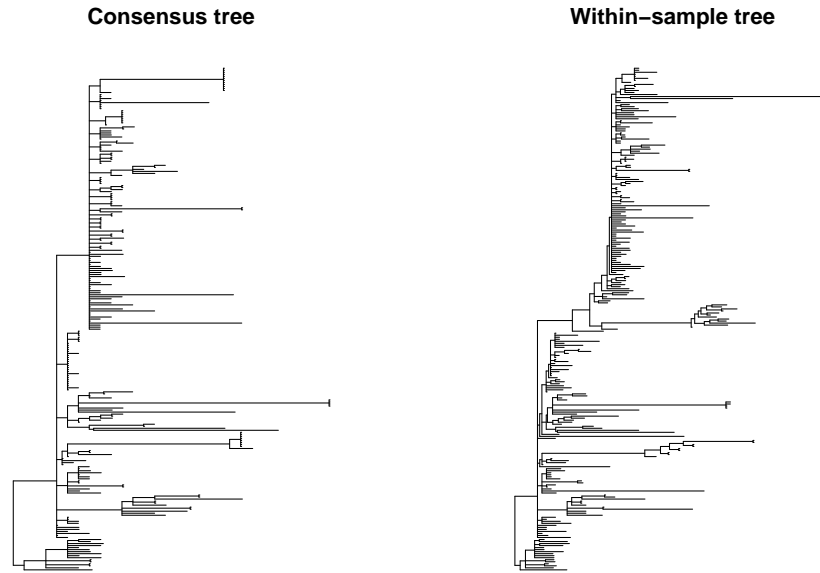
Supplementary Figure 4: Proportion of shared mixed variants between duplicated samples using different filters of allele frequency.

Individual plots of shared within-host variants between technical duplicates using increasing thresholds of allele frequency. Colors represent C_t value, while the size of the point shows the total number of within-host variants between the two samples.



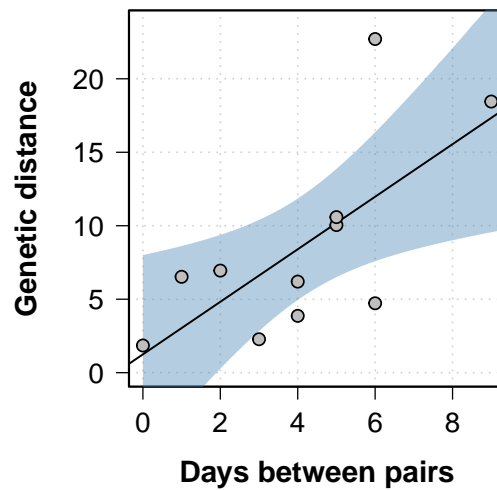
Supplementary Figure 5: Probability that mixed variants are shared.

Probability that low frequency variants are shared inferred with a logistic model with allele frequency and epidemiological relationship as independent variable and whether a variant is shared or not as dependent variable. Y-axis in logarithmic scale for representation.



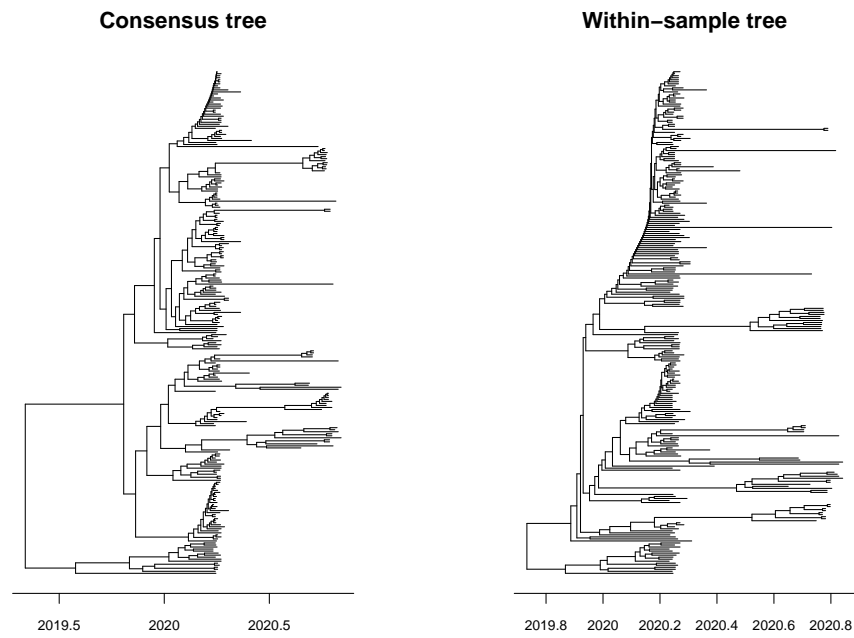
Supplementary Figure 6: Phylogenetic trees for SARS-CoV-2.

SARS-CoV-2 phylogenetic trees inferred from consensus sequences (left) and an alignment with major and minor variant information (right) .



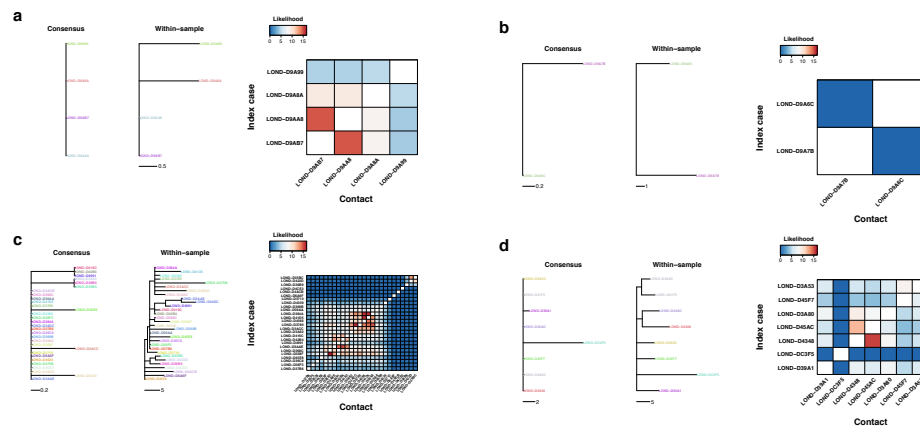
Supplementary Figure 7: Genetic distance between longitudinal samples.

The genetic distance in the phylogenetic tree inferred using within-sample diversity increased as the between longitudinal samples progressed. Black line shows the best fit in a linear model, while the blue shaded area represents the 95% CI.



Supplementary Figure 8: Time calibrated phylogenetic trees for SARS-CoV-2.

SARS-CoV-2 phylogenetic trees inferred from consensus sequences (left) and an alignment with major and minor variant information (right). Branch lengths are measured in years.



Supplementary Figure 9: Phylogenetic and transmission for SARS-CoV-2 outbreaks.

a-d Phylogenies of SARS-CoV-2 outbreaks. The branch lengths are in units of substitutions per genome, and the scales are shown under the trees. Colors represent samples from the same individual. Samples with the same name are technical replicates. Left tree of each panel shows the phylogeny inferred with the consensus alignment. Right tree represents the phylogeny inferred using within-sample variation. Heatmap shows the likelihood of direct transmission for each pair of samples in a SEIR model of transmission. Vertical axis is the infector while the horizontal axis shows the infectee.